Methodology and Computing in Applied Probability manuscript No.
(will be inserted by the editor)

A Stochastic Model for Multi-Hierarchical Networks

David Neuhäuser · Christian Hirsch · Catherine Gloaguen · Volker Schmidt

Received: date / Accepted: date

Abstract We provide a stochastic modelling approach for multi-hierarchical fixed-access telecommunication networks where cables are installed along the underlying road system. It constitutes an extension of network models consisting of only two hierarchy levels. We consider the effects of the introduction of an additional level of hierarchy on two functionals relevant in telecommunication networks, namely typical shortest-path lengths and total fibre lengths. Intuitively speaking, in the extended scenario, the typical shortest-path length gets longer whereas the total fibre length decreases. Both theoretical and numerical results are provided. The underlying infrastructure is assumed to be represented by a STIT tessellation which is particularly suitable for stochastic modelling of multi-hierarchical fixed-access telecommunication networks. In this context, we present a description of the Palm version of a planar STIT tessellation and give an appropriate simulation algorithm.

Keywords STIT tessellation · Palm version · multi-hierarchical networks · typical shortest-path · total fibre length · limit theorem · network planning

Mathematics Subject Classification (2000) 60D05, 65C05, 65C50

D. Neuhäuser, V. Schmidt
Ulm University, Institute of Stochastics
Helmholtzstrasse 18, 89069 Ulm, Germany
Tel.: +49 731 50 23555
E-mail: david.neuhaeuser@uni-ulm.de

C. Hirsch
Weierstrass Institute for Applied Analysis and Stochastics
Mohrenstrasse 39, 10117 Berlin, Germany
Tel.: +49 30 20372 478

C. Gloaguen
Orange Labs
38-40 rue du General Leclerc, 92794 Issy-Moulineaux Cedex 9, France
Tel.: +33 1 45 29 64 41

1 Introduction

During the last decade, the *Stochastic Subscriber Line Model* (SSLM) has been developed as a powerful and reliable stochastic modelling approach to investigate fixed-access telecommunication networks, see e.g. [4,5,13,16]. In the SSLM, high-level components (HLC) are located along the edges of a road graph and each of them is dedicated to providing service to all low-level components (LLC) in some bounded region of the plane. This area is referred to as its serving zone. Physical links from LLC to the relevant HLC are deployed along the shortest Euclidean path in the road graph which is modelled by a stationary random planar tessellation. Thus, the SSLM models a two-levels network architecture deployed on the road infrastructure in cities but also rural regions. However, large-scale fixed-access networks typically consist of more than one level of hierarchy. From a practical point of view, the introduction of an additional level of hierarchy offers the potential of substantially reducing total fibre lengths. Indeed, instead of requiring a fibre to a distant HLC, LLC now have the possibility to connect to a much closer network component in an intermediate level.

More generally speaking, by suitable superpositions and juxtapositions of such elementary two-levels building blocks or 'bricks', one can provide realistic models at country scale, taking into account its geographic and demographic features. The parametric description of the SSLM offers the possibility to deal with the fact that the population distribution is spatially inhomogeneous. Subnetworks for cities and rural areas are designed by simple adjustments of the parameters. The overall probabilistic results for geometry-dependent functionals (e.g. the probability density for the total connection length from the customer to the upper level node) are averages with a weighting dependent on the number of customers. The subnetworks may involve purely hierarchical n-levels networks which are the superposition of $n-1$ two-levels bricks. Then, in the process described above, the probability density functions for connection lengths are computed as convolutions of the corresponding parametric densities from each of the involved bricks, assuming pairwise statistical independence between them. This has not formally been proven yet, but the methodology has been successfully applied to the existing French copper network. The accuracy of the results is compatible with the real dataset. The combination of several building blocks with each other may be more risky if one deals with more complex functionals such as capacity trees. In that case, one is interested in the joint behaviour of several connections in a given serving zone (so-called multipoint to point view). At each location of an LLC, a given capacity (i.e. number of copper fibres or optical fibres, depending on the technology) joins the network and follows the shortest path to the respective HLC along the road system. Each street segment in the serving zone then supports a capacity depending on the geometry of the road system, on the number and locations of the LLC and on their incoming capacity. In a three-levels architecture, an HLC of the lower brick can be considered as an LLC in the higher brick and its capacity is itself a random quantity. A possible replacement by a deterministic, averaged value and its impact on the characteristics of the capacity tree is an open question. This motivates the stochastic analysis of three-levels networks presented in this paper. Moreover, the SSLM has considered so far the classical tessellation models (namely, Poisson-Delaunay tessellations, Poisson-Voronoi tessellations and Poisson line tessellations). Recently, the family of so-called STIT tessellations has

been thoroughly introduced and investigated, see [9,11,14,15,17]. STIT means "iteration stable tessellation" and seems to be a suitable stochastic model for road systems in cities since on the one hand, it reflects natural processes in city morphogenesis [2] and on the other hand, it provides an excellent fit to real street systems. For a general methodology to assess the quality of fit of models for street systems to real data, see [6].
The rest of this paper is organised as follows. In Section 2, we provide a precise definition of the multi-hierarchical extension of the SSLM where intermediate components are installed as an additional level of hierarchy. For this purpose, the necessary tools from stochastic geometry and their properties are presented. In particular, STIT tessellations and Cox processes with intensity measures concentrated on the edge system of such random tessellations are considered. Moreover, to rigorously introduce the notion of typical HLC or LLC, we recall some basic results from Palm theory for stationary point processes. Similarly, for a stationary tessellation, its Palm version can be regarded as a conditional variant of the tessellation obtained by putting the origin $o \in \mathbb{R}^2$ at random on its edge set. This corresponds to seeing the original tessellation from the point of view of an access point in the telecommunication network located at the origin. Section 3 deals with representation formulas for the distribution of various typical distances between LLC and HLC measured along the underlying edge system, i.e. so-called typical shortest-path lengths. These formulas are useful to derive the corresponding density functions of such random variables, for instance. Besides, we derive formulas for the expectation of typical total fibre lengths in the network, i.e., the total length of all fibres needed in order to connect each LLC in the typical serving to the corresponding HLC. Then, in Section 4 we provide a description for the Palm version of an isotropic STIT tessellation. It can be used for the implementation of an appropriate simulation algorithm for such random geometric graphs containing the origin on their edge set with probability one. Based on this algorithm, in Section 5 we provide numerical results illustrating the distributional behaviour of various typical shortest-path lengths and total fibre lengths. Furthermore, in Section 6, we derive the limit distributions of such typical shortest-path lengths if the linear intensity of the HLC tends to infinity. Moreover, we give a formal proof for the observation that connecting LLC to HLC via intermediate level components causes on the one hand a longer path connection length but – for a sufficiently high linear intensity of the LLC – a decrease in the total fibre length of the telecommunication network, as well. Finally, Section 7 concludes the paper and gives an outlook to possible future research.

2 Stochastic Modelling Approach

The goal of this section is to provide a precise definition of the multi-hierarchical extension of the SSLM. In order to adapt the SSLM accordingly, we propose two additional modelling features. First, the network components of different levels of hierarchy are placed on disjoint edge sets of the underlying tessellation representing the infrastructure. For instance, considering STIT tessellations, HLC are placed on long edges while LLC are located on rather short edges. Then, as a third level of hierarchy, we introduce the notion of intermediate level components. Recall

that the SSLM consists of three modelling layers, namely the geometry model, the network model and the topology model. They read as follows, see also [12].

2.1 The Geometry Model

The underlying road system along which the cables of a telecommunication network are assumed to be installed has been modelled by classical tessellation models so far, i.e. Poisson-Delaunay tessellations, Poisson-Voronoi tessellations and Poisson line tessellations, see for instance [12,16]. In the present paper, we extend this class of random geometric graphs by stationary tessellations which are stable with respect to iteration, so-called STIT tessellations, see e.g. [11,14,15,17]. This type of random tessellations is particularly well-suited for modelling multi-hierarchical networks since it exhibits large variations of edge lengths. For instance, rather long line segments can be thought to represent the main roads of the road system, see the green lines on the right in Figure 1. Note that in the context of STIT tessellations, the edges are also called I-segments.

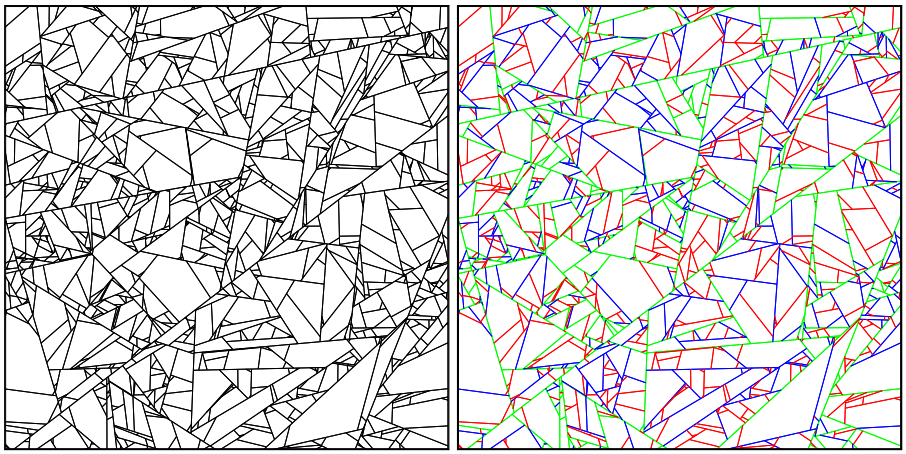

Fig. 1 STIT tessellation (left) and colouring of its edges (right) according to their arrival times where the green edges arrive in the first arrival period, the blue edges in the second period and the red edges in the third period

2.1.1 STIT Tessellations in $\mathbb{R}^2$

For a better understanding of the technical details in the present paper, we briefly recall the definition of a stationary STIT tessellation T in $\mathbb{R}^2$. For any stationary random tessellation $T_0 = \{\Xi_i\}_{i\geq 1}$ and an iid sequence $\mathcal{T} = (T_1, T_2, \ldots)$ of stationary random tessellations independent of T_0, the nesting operation yields a new tessellation $\tau(T_0|\mathcal{T}) = \tau(T_0|T_1, T_2, \ldots) = \bigcup_{i=1}^{\infty}(\Xi_i \cap T_i)$, where Ξ_i is the i-th cell of T_0. Thus, for each cell Ξ_i an elementwise intersection with the elements of T_i is performed. In order to define a STIT tessellation formally, we need

a sequence $\{\tau_n(T_0)\}_{n\geq 2}$ of rescaled iterations given by $\tau_2(T_0) = \tau(2T_0|2\mathcal{T}_1)$ and $\tau_n(T_0) = \tau(\frac{n}{n-1}\tau_{n-1}(T_0)|n\mathcal{T}_{n-1})$ for $n \in \{3,4,\ldots\}$. Here, $\mathcal{T}_1, \mathcal{T}_2, \ldots$ denotes a sequence of tessellation sequences such that all involved tessellations are iid (including the stationary tessellation T_0). Then, a stationary random tessellation T is called a STIT tessellation if

$$T \stackrel{\mathrm{d}}{=} \tau_n(T) \text{ for all } n \in \{2,3\ldots\}.$$

According to [10], it is equivalent to define the STIT property by $T \stackrel{\mathrm{d}}{=} \tau_2(T)$. Note that the rescaling factor n is needed in order to preserve the same length intensity for each tessellation $\tau_n(T)$. The existence of STIT tessellations is shown in [11].

2.1.2 Construction of STIT Tessellations in Compact and Convex Sets

In this section, we recall a method in order to construct the restriction of a STIT tessellation T with edge length intensity $\gamma > 0$ in a compact and convex set $W \subset \mathbb{R}^2$ with non-empty interior, since it is used in Section 4 of the present paper. Note in particular that $\gamma = \mathbb{E}\,\nu_1(T^{(1)} \cap [0,1]^2)$, where $T^{(1)}$ denotes the corresponding edge set of T.

Let Q_1 be a probability measure on the space $\mathbb{A}_o$ of all lines in $\mathbb{R}^2$ through the origin $o \in \mathbb{R}^2$ such that for any line $\ell \in \mathbb{A}_o$, $Q_1(\{\ell\}) < 1$. Besides we denote by Q_2 the induced translation invariant measure on the space $\mathbb{A} = \mathbb{R}^2 \times \mathbb{A}_o$ of all lines in $\mathbb{R}^2$ which is given by $dQ_2(s,t) = ds\, Q_1(dt)$. Let $\{\ell_i, \theta_i\}_{i\geq 1}$ be an iid sequence of pairs of independent random variables, where $\ell_i \in \mathbb{A}$ and $\theta_i \in (0,\infty)$ are distributed as follows. The random lines $\{\ell_i\}_{i\geq 1}$ are distributed according to the normalised measure $\frac{Q_2(\cdot \cap \{\ell \in \mathbb{A}:\, \ell \cap W \neq \emptyset\})}{Q_2(\{\ell \in \mathbb{A}:\, \ell \cap W \neq \emptyset\})}$ and the random variables $\{\theta_i\}_{i\geq 1}$ are exponentially distributed with parameter $Q_2(\{\ell \in \mathbb{A} :\, \ell \cap W \neq \emptyset\})$. Throughout this paper, we assume Q_1 to be the uniform distribution on $\mathbb{A}_o$ and thus, $Q_2(\{\ell \in \mathbb{A} :\, \ell \cap W \neq \emptyset\}) = p_W/\pi$, where p_W denotes the perimeter of W. The restriction $T \cap W$ of the STIT tessellation T to the compact and convex sampling window W is obtained in the following way, see e.g. [7].

(i) If $\theta_1 > \gamma$, the construction is stopped and the resulting tessellation is just W (i.e., no edges of the tessellation to be constructed are present within W).
(ii) Otherwise, if $\theta_1 \leq \gamma$, the line ℓ_1 splits W into two sub-windows W_+ and W_-. These are then treated in the following way, separately and independently.
   (a) If $\theta_1 + \theta_2 > \gamma$, then W_+ remains as it is and will be a part of the final tessellation.
   (b) If $\theta_1 + \theta_2 \leq \gamma$ and ℓ_2 hits W_+, then W_+ is divided by the line ℓ_2 into two new sets, say W_{++} and W_{+-}. In this case, the procedure continues with W_{++} and W_{+-}. Otherwise, the next possible division of W_+ is at time $\theta_1 + \theta_2 + \theta_3$ if $\theta_1 + \theta_2 + \theta_3 \leq \gamma$.
   (c) Accordingly, steps (a) and (b) are carried out for W_- with corresponding (ℓ_i, θ_i) which are independently sampled from those used for W_+.

According to this construction principle of the restriction $T \cap W$ of the STIT tessellation T to the sampling window W, each line ℓ_i which subdivides a convex set into two new convex sets is marked with its so-called arrival time θ_i. Furthermore, from the construction principle stated above, it follows that in the isotropic case the distribution of the STIT tessellation T is completely characterised by the single parameter $\gamma > 0$.

2.2 The Network Model

In the standard SSLM [16], the network components are represented by two conditionally independent Cox processes given the underlying tessellation T, say $X_H = \{X_{H,n}\}_{n\geq 1}$ (for the HLC) and $X_L = \{X_{L,n}\}_{n\geq 1}$ (for the LLC). Their random intensity measures are concentrated on the edge set $T^{(1)}$ of T. Thus, given T and the total number of points on $T^{(1)} \cap W$, both types of components are uniformly distributed on the entire edge set of $T^{(1)} \cap W$ for each bounded Borel set $W \in \mathcal{B}(\mathbb{R}^2)$ with non-empty interior. In the present paper, we modify this scenario as follows.

Consider three levels of hierarchy by introducing a third Cox process $X_I = \{X_{I,n}\}_{n\geq 1}$ of intermediate level components (ILC) whose random intensity measure is again concentrated on the edge set of T. However, now we make a more detailed use of the structure of the STIT tessellation. We subdivide $T^{(1)}$ into three types of stationary edge sets, say $T_H^{(1)}$ (green segments), $T_I^{(1)}$ (blue segments) and $T_L^{(1)}$ (red segments), cf. Figure 1, with corresponding length intensities $\gamma^H, \gamma^I, \gamma^L > 0$ such that $\gamma^H + \gamma^I + \gamma^L = \gamma$. To be more precise, a line segment with arrival time θ belongs to $T_H^{(1)}$ if $\theta \in [0, \gamma^H]$, to $T_I^{(1)}$ if $\theta \in (\gamma^H, \gamma^H + \gamma^I]$ and to $T_L^{(1)}$ if $\theta \in (\gamma^H + \gamma^I, \gamma]$. Thus, with probability one, we have for $i, j \in \{H, I, L\}$, $i \neq j$ that $T_i^{(1)} \cap T_j^{(1)}$ is the empty set or consists of at most countably many points. Besides, $T_H^{(1)} \cup T_I^{(1)} \cup T_L^{(1)} = T^{(1)}$. Note that the length intensities of these three edge sets are given by $\gamma^H = \mathbb{E}\,\nu_1(T_H^{(1)} \cap [0,1]^2)$, $\gamma^I = \mathbb{E}\,\nu_1(T_I^{(1)} \cap [0,1]^2)$ and $\gamma^L = \mathbb{E}\,\nu_1(T_L^{(1)} \cap [0,1]^2)$. According to [10], these intensities can be computed explicitly. Then, in contrast to the standard SSLM where HLC for any bounded Borel set $W \in \mathcal{B}(\mathbb{R}^2)$ are conditionally uniformly distributed on the entire edge set $T^{(1)} \cap W$, we assume the points of the Cox process X_H inside W to be located conditionally uniformly on $T_H^{(1)} \cap W$. Analogously, we assume the points of X_I to be located on $T_I^{(1)}$ and those of X_L on $T_L^{(1)}$. In particular, it holds that $\mathbb{E}X_i(B) = \lambda_\ell^i\, \mathbb{E}\nu_1(B \cap T_i^{(1)})$ for some linear intensity $\lambda_\ell^i > 0$, any Borel set $B \in \mathcal{B}(\mathbb{R}^2)$ and $i \in \{H, I, L\}$ where ν_1 denotes the one-dimensional Hausdorff measure in $\mathbb{R}^2$. Note for instance that by this construction, the points of the highest level of hierarchy, i.e. HLC, will be put on $T_H^{(1)}$, which consists of those lines in the STIT tessellation which have arrived before time γ^H. Furthermore, we assume that the point processes X_H, X_I and X_L are conditionally independent given $T_H^{(1)}$, $T_I^{(1)}$ and $T_L^{(1)}$.

2.3 The Topology Model

Equipped with a suitable model for the underlying road system and the network components, we can now proceed in terms of connection rules within the SSLM, i.e. defining in which way network components are associated with one another. In order to define such links, serving zones have played a crucial role so far when investigating networks with just two levels of hierarchy, see e.g. [13]. This methodology can be adapted to the framework considered in the present paper as follows.

Consider the *graph-based* Voronoi tessellation $\{S_n\}_{n\geq 1}$ with nuclei $\{X_{H,n}\}_{n\geq 1}$ given by

$$S_n = \{x \in T^{(1)} : c(x, X_{H,n}) \leq c(x, X_{H,m}) \text{ for all } m \geq 1\},$$

where $c(x, X_{H,n})$ denotes the length of the shortest path from $x \in T^{(1)}$ to $X_{H,n}$ along the edge system of the underlying tessellation. As such, $\{S_n\}_{n\geq 1}$ associates to each point $X_{H,n}$ a serving zone S_n (which corresponds to the grey subset of $T^{(1)}$ in Figure 2).

Concerning the connection rules for an LLC $X_{L,k}$ of X_L lying within S_n, we distinguish two scenarios. In scenario 1, no ILC are allowed and the LLC are always directly connected to HLC. The difference to the standard SSLM is simply the placement of network components along the underlying infrastructure. In scenario 2 however, ILC are explicitly desirable and we proceed in the following way, cf. Figure 2. If an ILC $X_{I,m} \in S_n$ is in the graph sense closer to $X_{L,k}$ than the nucleus $X_{H,n}$ of S_n, then we connect $X_{L,k}$ to $X_{H,n}$ indirectly via $X_{I,m}$ (left-hand side of Figure 2). Otherwise, we connect $X_{L,k}$ directly to $X_{H,n}$ (centre of Figure 2) along $T^{(1)}$. Besides, we link an ILC $X_{I,m}$ of X_I which is located inside S_n to $X_{H,n}$ via the shortest possible path measured along $T^{(1)}$, see right-hand side of Figure 2. Note that in purely hierarchical networks of scenario 2, LLC will always be indirectly connected to their respective HLC via the corresponding ILC. Nevertheless, we choose our connection rules as defined for the sake of rigorous mathematical proofs provided in the paper.

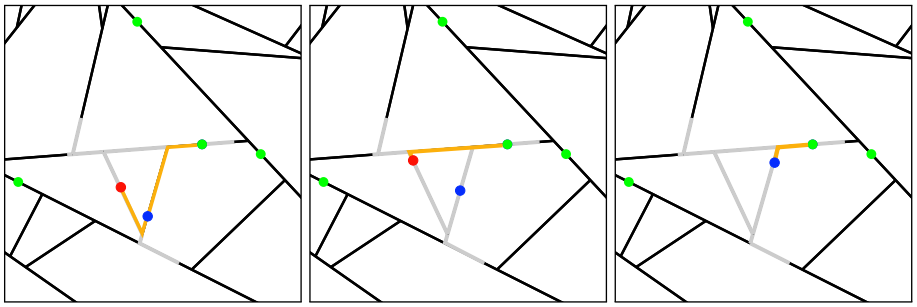

Fig. 2 Paths of connection rules for scenario 2 (orange): between LLC in red and HLC in green indirect via ILC in blue (left), direct (centre), and connection between ILC and HLC (right)

2.4 Some Palm Calculus and the Typical Cell

When investigating large telecommunication networks, one faces the problem that not only a few but quite many serving zones occur in the relevant area. This in turn makes the investigation of functionals relevant in telecommunication networks a very time-consuming matter. One successful and reliable way out of this problem has been the usage of Palm calculus and typical cells, see [4,5,13], which can be

successfully adapted to the scenario of the present paper. Due to the nature of the functionals which we want to investigate, we need to consider typical points with respect to two different Palm measures. On the one hand, for typical shortest-path lengths, we are interested in the length of a (possibly indirect) path from a typical LLC to its associated HLC. On the other hand, the typical total fibre length in the serving zones of the network is computed from the point of view of a typical HLC. This requires some technical efforts. Sections 2.4.1 and 2.4.2 provide an appropriate framework by using Palm calculus. Additional information on Palm distributions can be found e.g. in [1] and [3].

2.4.1 Palm Calculus with Respect to LLC

First, we define the Palm version $\widetilde{X}_L$ of X_L with respect to LLC. Its distribution can be seen as the conditional distribution of X_L given that there is an LLC located at the origin $o = (0,0) \in \mathbb{R}^2$. More precisely, the following representation formula allows for a description of the distribution of $\widetilde{X}_L$. For an arbitrary measurable function $f : \mathbb{L} \to [0,\infty)$, we have

$$\mathbb{E} f(\widetilde{X}_L) = \frac{1}{\lambda^L}\, \mathbb{E} \sum_{i:\, X_{L,i} \in [0,1]^2} f(\{X_{L,n}\} - X_{L,i})\,,$$

where $\lambda^L = \lambda_\ell^L \gamma^L$. Here, $\mathbb{L}$ denotes the family of all locally finite sets of $\mathbb{R}^2$ equipped with the σ-algebra $\mathcal{L}$ such that the function which maps $\varphi \in \mathbb{L}$ to $\#\varphi \cap B$ (the cardinality of the set $\varphi \cap B$) is measurable for each $B \in \mathcal{B}(\mathbb{R}^2)$. Similarly, the Palm version $\widetilde{X}_H$ of X_H with respect to LLC is given by

$$\mathbb{E} f(\widetilde{X}_H) = \frac{1}{\lambda^L}\, \mathbb{E} \sum_{i:\, X_{L,i} \in [0,1]^2} f(\{X_{H,n}\} - X_{L,i})\,.$$

The Palm version $\widetilde{X}_I$ of X_I with respect to LLC can be defined analogously.

In order to investigate distributional properties of typical shortest-path lengths via simulations, it is often useful to consider the Palm version $\widetilde{T}$ of the underlying tessellation T with respect to $\nu_1(\cdot \cap T_L^{(1)})$. Again, the distribution of $\widetilde{T}$ can be interpreted as the distribution of T under the condition that the origin o belongs to the edge set $T_L^{(1)}$. More precisely, for an arbitrary measurable function $h : \mathbb{T} \to [0,\infty)$, we have

$$\mathbb{E} h(\widetilde{T}) = \frac{1}{\gamma^L}\, \mathbb{E} \int_{T_L^{(1)} \cap [0,1]^2} h(T - x)\, \nu_1(dx)\,,$$

where $\mathbb{T}$ denotes the family of all tessellations in $\mathbb{R}^2$. Since tessellations can be identified with their respective edge sets, the corresponding σ-algebra is given by the trace of the hitting σ-algebra on $\mathbb{T}$, see [1]. Note that $\widetilde{X}_H$ can be considered as a Cox process whose random intensity measure is concentrated on $\widetilde{T}$, see [13].

2.4.2 Palm Calculus with Respect to HLC

Next, we consider Palm distributions with respect to HLC. In principle, one can proceed in the same way as in Section 2.4.1. For instance, the Palm version X_H^* of X_H with respect to HLC is characterised by the representation formula

$$\mathbb{E}f(X_H^*) = \frac{1}{\lambda^H}\,\mathbb{E}\sum_{i:\,X_{H,i}\in[0,1]^2} f(\{X_{H,n}\}-X_{H,i})\,,$$

where $f:\mathbb{L}\to[0,\infty)$ is an arbitrary measurable function. The point processes X_I^*, X_L^* and the tessellation T^* are defined correspondingly. This terminology leads us to the definition of the typical serving zone S^* which is the typical (Cox-)Voronoi cell of X_H defined as the zero-cell of the graph-based Voronoi tessellation induced by X_H^*, i.e.,

$$S^* = \{x\in T^*:\, c(x,o)\le c(x,X_{H,m}^*) \text{ for all } m\ge 1\}\,.$$

By $Z^* = \{Z_i^*\}_{1\le i\le M}$, we denote the set of M points consisting of the HLC located in o and all ILC located on S^*. According to the connection rules in the topology model described in Section 2.3, the set of network nodes Z^* decomposes S^* into several sub-serving zones. They are defined as the graph-based Voronoi cells $\{R_i^*\}_{1\le i\le M}$ given by

$$R_i^* = \{x\in S^*: c(x,Z_i^*)\le c(x,Z_j^*) \text{ for all } 1\le j\le M\}.$$

For an illustration of the situation, see Figure 3. Moreover, we write $S_L^* = S^*\cap T_L^{*(1)}$ and $R_{L,i}^* = R_i^*\cap T_L^{*(1)}$ for the subsets of the edge sets S^* and R_i^* where only LLC are located on. Here, $T_L^{*(1)}$ denotes the subset of all edges in T^* whose arrival time is contained in $(\gamma^H+\gamma^I,\gamma]$.

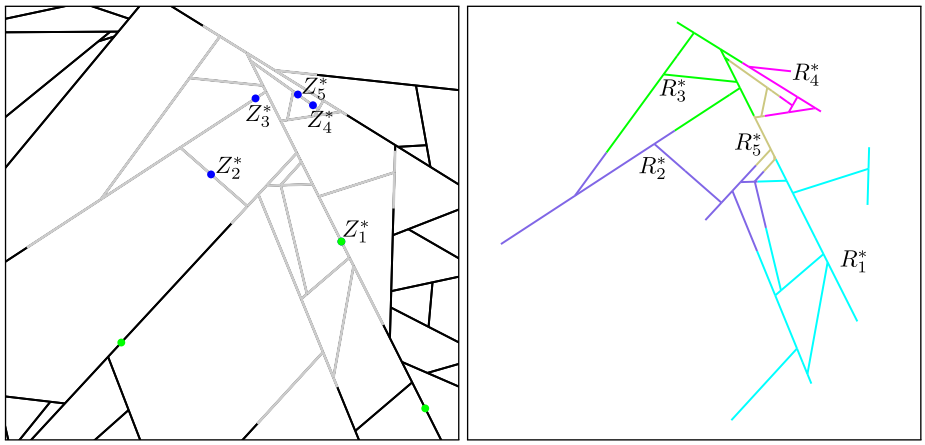

Fig. 3 Typical serving zone S^* (grey) and network nodes $\{Z_i^*\}_{1\le i\le M}$ (left), as well as corresponding subdivision into Voronoi cells $\{R_i^*\}_{1\le i\le M}$ (right)

3 Typical Shortest-path Lengths and Total Fibre Lengths

In the present paper, we consider two types of functionals which are relevant in telecommunication networks. The first one deals with various typical distances measured along the underlying infrastructure. The second one treats typical total fibre lengths in the network. In the following, we give precise descriptions of these quantities.

3.1 Typical Shortest-path Lengths

In order to optimise costs in fixed-access telecommunication networks, one important aspect is to minimise the fibre length required for the connections between network components. In the following, we therefore investigate the distributional behaviour of shortest-path lengths in two scenarios. On the one hand, we are interested in the distribution of the random variable $\widetilde{C}_{LH} = c(o, \widetilde{X}_{H,o})$, where $\widetilde{X}_{H,o}$ denotes the closest point in the graph sense of $\widetilde{X}_H$ to the LLC located at o. This means that $\widetilde{C}_{LH}$ is the length of the shortest path from o to the respective node of $\widetilde{X}_H$ along $\widetilde{T}^{(1)}$. On the other hand, we investigate the random variable $\widetilde{C}_{LIH} = c(o, \Phi) + c(\Phi, \widetilde{X}_{H,o})$, where Φ denotes the closest point in graph sense to o among $\widetilde{X}_{H,o}$ and all ILC inside the serving zone corresponding to $\widetilde{X}_{H,o}$. That is, $\widetilde{C}_{LIH}$ is the shortest-path length of the (possibly indirect via an ILC) connection from o to $\widetilde{X}_{H,o}$ running along $\widetilde{T}^{(1)}$. In the following theorem, we state representation formulas for the distribution of the typical shortest-path lengths $\widetilde{C}_{LH}$ and $\widetilde{C}_{LIH}$. These formulas express quantities defined using the Palm distribution of the LLC in terms of quantities defined using the Palm distribution of the HLC. In particular, then, an HLC is located at the origin.

Theorem 1 *Let $h : [0, \infty) \to [0, \infty)$ be any measurable function. Then,*

$$\mathbb{E}\, h(\widetilde{C}_{LH}) = \frac{1}{\mathbb{E}\, \nu_1(S_L^*)}\, \mathbb{E} \int_{S_L^*} h(c(o, y))\, \nu_1(dy). \tag{1}$$

Furthermore, it holds that

$$\mathbb{E}\, h(\widetilde{C}_{LIH}) = \frac{1}{\mathbb{E}\, \nu_1(S_L^*)}\, \mathbb{E} \int_{S_L^*} h(c(o, g(y)) + c(g(y), y))\, \nu_1(dy), \tag{2}$$

where $g(y)$ denotes the closest point in graph sense to y among the HLC in o and all ILC inside S^*.

Proof Formula (1) can be obtained in a similar way as formula (5) in [16] where a representation formula for the distribution of typical point-to-point distances has been derived for a related scenario. This was achieved by using Neveu's exchange formula for jointly stationary marked point processes, see e.g. [8]. Therefore, we focus on the case considered in (2). Let $\mathcal{F}^o$ denote the family of finite segment systems containing the origin o and define the function $f : \mathbb{R}^2 \times [0, \infty) \times \mathcal{F}^o \to [0, \infty)$ by $f(x, c, \xi) = h(c)\mathbb{1}_{\xi + x}(o)$. Besides, let $\widetilde{S}_n^o$ denote the serving zone associated with $\widetilde{X}_{H,n}$ shifted to o. Furthermore, we write $C^*_{HIL,n}$ for the (possibly indirect via an ILC) connection length from $X^*_{L,n}$ to its associated HLC. Then,

$$\begin{aligned}\mathbb{E}\, h(\widetilde{C}_{LIH}) &= \mathbb{E}\sum_{n\geq 1} f(\widetilde{X}_{H,n}, \widetilde{C}_{LIH}, \widetilde{S}_n^o)\\ &= \frac{\lambda^H}{\lambda^L}\,\mathbb{E}\sum_{n\geq 1} f(-X_{L,n}^*, C_{HIL,n}^*, S^*)\\ &= \frac{\lambda^H}{\lambda^L}\,\mathbb{E}\sum_{n\geq 1} h(C_{HIL,n}^*)\,\mathbb{1}_{S^*}(X_{L,n}^*),\end{aligned}$$

where the second equality is obtained by applying Neveu's exchange formula. Recalling the definition of conditional expectation leads to

$$\begin{aligned}&\frac{\lambda^H}{\lambda^L}\,\mathbb{E}\sum_{n\geq 1} h(C_{HIL,n}^*)\,\mathbb{1}_{S^*}(X_{L,n}^*)\\ =\ &\frac{\lambda^H}{\lambda^L}\,\mathbb{E}\Big(\mathbb{E}\Big(\sum_{X_{L,n}^*\in S_L^*} h\left(c\left(o, g(X_{L,n}^*)\right) + c\left(g(X_{L,n}^*), X_{L,n}^*\right)\right) \,\Big|\, S_L^*, X_I^*\Big)\Big).\end{aligned}$$

An application of Campbell's theorem (see e.g. [1]) yields

$$\begin{aligned}&\frac{\lambda^H}{\lambda^L}\,\mathbb{E}\Big(\mathbb{E}\Big(\sum_{X_{L,n}^*\in S_L^*} h\left(c\left(o, g(X_{L,n}^*)\right) + c\left(g(X_{L,n}^*), X_{L,n}^*\right)\right) \,\Big|\, S_L^*, X_I^*\Big)\Big)\\ =\ &\frac{\lambda^H}{\lambda^L}\,\mathbb{E}\,\lambda_\ell^L \int_{S_L^*} h(c(o, g(y)) + c(g(y), y))\,\nu_1(dy)\\ =\ &\frac{\lambda_\ell^H \gamma^H}{\lambda_\ell^L \gamma^L}\,\mathbb{E}\,\lambda_\ell^L \int_{S_L^*} h(c(o, g(y)) + c(g(y), y))\,\nu_1(dy).\end{aligned}$$

Finally, putting $h(\cdot) = 1$ yields $\gamma^L = \lambda_\ell^H \gamma^H\,\mathbb{E}\,\nu_1(S_L^*)$, which completes the proof.

Remark 1 At first glance, it may be counterintuitive that formulas for typical characteristics with respect to LLC are given in terms of the Palm distribution with respect to HLC. However, this is just the benefit of Neveu's exchange formula.

Naturally, splitting $\Psi \in \{S^*, R_i^*,\ i \in \{1,\dots,M\}\}$ at its respective crossings, endings and distance-peaks into segments (cf. [16] for more information) yields a subdivision of $\Psi_L \in \{S_L^*, R_{L,i}^*, i \in \{1,\dots,M\}\}$. The edges of Ψ_L with starting points $A_j(\Psi_L)$ and end points $B_j(\Psi_L)$ will be denoted by $E_j(\Psi_L)$ in the following. They are designed in a way such that they satisfy the following conditions. First, $\Psi_L = \bigcup_{j=1}^{N(\Psi_L)} E_j(\Psi_L)$. Second, $\nu_1(E_j(\Psi_L) \cap E_k(\Psi_L)) = 0$ for $j \neq k$ and finally, $c(o, A_j(\Psi_L)) < c(o, A_j(\Psi_L)) + \nu_1(E_j(\Psi_L)) = c(o, B_j(\Psi_L))$.. In order to derive the density functions of $\widetilde{C}_{LH}$ and $\widetilde{C}_{LIH}$, we use the following terminology. Let f'_{Ψ_L} : $[0,\infty) \times [0,\infty) \to \mathbb{N}_0$ be defined as

$$f'_{\Psi_L}(x,z) = \sum_{i=1}^{N(\Psi_L)} \mathbb{1}_{[c(z,A_i(\Psi_L)),c(z,B_i(\Psi_L)))+c(o,z)}(x).$$

Then, the following result can be shown using the same arguments as in the two-level scenario, [16, Theorem 1]. Nevertheless, for the convenience of the reader, we present a detailed proof.

Corollary 1 *The density functions* $f_{\widetilde{C}_{LH}} : [0,\infty) \to [0,\infty)$ *of* $\widetilde{C}_{LH}$ *and* $f_{\widetilde{C}_{LIH}} : [0,\infty) \to [0,\infty)$ *of* $\widetilde{C}_{LIH}$ *are given by*

$$f_{\widetilde{C}_{LH}}(x) = \frac{1}{\mathbb{E}\,\nu_1(S_L^*)}\,\mathbb{E} f'_{S_L^*}(x,o) \tag{3}$$

and

$$f_{\widetilde{C}_{LIH}}(x) = \frac{1}{\mathbb{E}\,\nu_1(S_L^*)}\,\mathbb{E}\sum_{i=1}^{M} f'_{R^*_{L,i}}(x, Z_i^*). \tag{4}$$

Proof Identities (3) and (4) are an immediate consequence of Theorem 1 by setting $h(x) = \mathbb{1}_B(x)$, $B \in \mathcal{B}(\mathbb{R})$. In particular, for (3) we have

$$\begin{aligned}
\mathbb{P}_{\widetilde{C}_{LH}}(B) &= \frac{1}{\mathbb{E}\,\nu_1(S_L^*)}\,\mathbb{E}\sum_{j=1}^{N(S_L^*)} \int_{c(o,A_j(S_L^*))}^{c(o,B_j(S_L^*))} \mathbb{1}_B(x)\,dx \\
&= \frac{1}{\mathbb{E}\,\nu_1(S_L^*)}\,\mathbb{E}\sum_{j=1}^{N(S_L^*)} \int_B \mathbb{1}_{[c(o,A_j(S_L^*)),c(o,B_j(S_L^*)))}(x)\,dx \\
&= \int_B \frac{1}{\mathbb{E}\,\nu_1(S_L^*)}\,\mathbb{E}\sum_{j=1}^{N(S_L^*)} \mathbb{1}_{[c(o,A_j(S_L^*)),c(o,B_j(S_L^*)))}(x)\,dx \\
&= \int_B \frac{1}{\mathbb{E}\,\nu_1(S_L^*)}\,\mathbb{E} f'_{S_L^*}(x,o)\,dx.
\end{aligned}$$

For showing (4), one can proceed analogously.

Remark 2 Note that S_L^* can be empty with positive probability, i.e., it holds that $\mathbb{P}(S_L^* = \emptyset) > 0$. In fact, we have $o \in T_H^{*(1)}$, where $T_H^{*(1)}$ denotes those edges in T^* whose arrival time is contained in $[0, \gamma^H]$. For some λ_ℓ^H sufficiently large, it can happen that $S^* \subset T_H^{*(1)}$ and thus $S_L^* = S^* \cap T_L^{*(1)} \subset T_H^{*(1)} \cap T_L^{*(1)} = \emptyset$.

Observe that the densities described in (3) and (4) are qualitatively different from these obtained in [16]. Indeed, in that paper it is shown that for a two levels scenario with HLC and LLC both located on the whole underlying random geometric graph and where the serving zones are defined as the *Euclidean* Voronoi cells induced by the the HLC, it holds that $f_{\widetilde{C}}(0) = 2\lambda_\ell$. In that context, $\widetilde{C}$ denotes the typical shortest path length and λ_ℓ the linear intensity of the HLC. Contrarily, in the situation of the present paper, we obtain from Corollary 1 that $f_{\widetilde{C}_{LH}}(0) = f_{\widetilde{C}_{LIH}}(0) = 0$.

3.2 Typical Total Fibre Lengths

Besides typical shortest-path lengths, total fibre lengths are another important functional in order to optimise fixed-access telecommunication networks in view of costs. In the present section, we are therefore interested in the distribution of the random variables D_{HL}^* as well as $D_{HIL,\alpha}^*$. Here, we denote by D_{HL}^* the sum

of the lengths of shortest paths along the edge set of T^* from the HLC in o to all nodes $X^*_{L,n}$ contained in the typical serving zone S^*. More precisely, we define

$$D^*_{HL} = \sum_{X^*_{L,n} \in S^*_L} c(o, X^*_{L,n}).$$

In other words, we assume that each LLC uses a separate fibre to connect to its associated HLC. When adding the third network layer, we still assume that each LLC needs a separate fibre to connect to its closest ILC. However, for the final part of the connection that goes from the ILC to the HLC, we assume that fibres can be gathered in bundles. In practice, fibres are gathered in cables and cabling policy is extremely complex to implement since real cables have predetermined sizes (i.e., the number of fibres included in a cable). In this paper, we consider a mathematically simplified model, where the total fibre length that is needed for the final part grows as a concave function in the number of the LLC that use this ILC. That is, for $\alpha \in [0,1]$ we put

$$D^*_{HIL,\alpha} = \sum_{i=1}^{M} \Big(c(o, Z^*_i) \cdot \big(\#(R^*_{L,i} \cap \{X^*_{L,m}\})\big)^{\alpha} + \sum_{X^*_{L,m} \in R^*_{L,i}} c(Z^*_i, X^*_{L,m}) \Big).$$

Thus, varying $\alpha \in [0,1]$ could mimic the complex cabling policies. On the one hand, for $\alpha = 1$, $D^*_{HIL,\alpha}$ represents the total length of the fibres from all LLC to HLC inside the typical serving zone, including the detour via corresponding ILC according to the connection rules of Section 2.3. This means that the length of a path from an ILC to HLC is added as often as the number of the respective LLC. On the other hand, the case where $\alpha = 0$ corresponds to adding the lengths of all LLC to ILC to the lengths of all ILC to HLC (each now counted once).
The total fibre lengths are conceptually more involved than the typical distances, as they take into account the shortest-path lengths corresponding to multiple lower-level nodes. Therefore, it seems difficult to derive an analogue of the distributional representation formula from Section 3.1 for total cable lengths. Still, one can obtain the following representation formulas for the respective first moments using the notation $\rho_\alpha(\beta) = \mathbb{E}X^\alpha$ for $X \sim \mathrm{Poi}(\beta)$.

Theorem 2 *It holds that*

$$\mathbb{E}D^*_{HL} = \mathbb{E}\,\lambda_\ell^L \int_{S^*_L} c(o,y)\,\nu_1(dy), \tag{5}$$

and furthermore

$$\mathbb{E}D^*_{HIL,\alpha} = \mathbb{E}\sum_{i=1}^{M} \Big(c(o, Z^*_i)\rho_\alpha(\lambda_\ell^L \nu_1(R^*_{L,i})) + \lambda_\ell^L \int_{R^*_{L,i}} c(y, g(y))\,\nu_1(dy) \Big). \tag{6}$$

Proof We start with the proof of (5). It holds that

$$\begin{aligned}
\mathbb{E}D^*_{HL} &= \mathbb{E} \sum_{X^*_{L,m} \in S^*_L} c(o, X^*_{L,m}) \\
&= \mathbb{E}\Big(\mathbb{E}\Big(\sum_{X^*_{L,m} \in S^*_L} c(o, X^*_{L,m}) \,\Big|\, S^*_L \Big) \Big) \\
&= \mathbb{E}\,\lambda_\ell^L \int_{S^*_L} c(o,y)\,\nu_1(dy),
\end{aligned}$$

where the latter equality is obtained by an application of Campbell's theorem. We proceed now with proving (6). It holds that

$$\begin{aligned}\mathbb{E}D^*_{HIL,\alpha} &= \mathbb{E}\sum_{i=1}^{M}\Big(c(o,Z_i^*)\cdot\big(\#(R^*_{L,i}\cap\{X^*_{L,m}\})\big)^{\alpha}+\sum_{X^*_{L,m}\in R^*_{L,i}}c(Z_i^*,X^*_{L,m})\Big)\\ &= \mathbb{E}\Big(\sum_{i=1}^{M}\mathbb{E}\Big(c(o,Z_i^*)\cdot\big(\#(R^*_{L,i}\cap\{X^*_{L,m}\})\big)^{\alpha}\\ &\quad+\sum_{X^*_{L,m}\in R^*_{L,i}}c(Z_i^*,X^*_{L,m})\,\big|\,R^*_{L,i},Z_i^*\Big)\Big)\\ &= \mathbb{E}\Big(\sum_{i=1}^{M}c(o,Z_i^*)\cdot\rho_\alpha(\lambda_\ell^L\nu_1(R^*_{L,i}))+\lambda_\ell^L\int_{R^*_{L,i}}c(g(y),y)\,\nu_1(dy)\Big)\end{aligned}$$

which completes the proof.

4 The Palm Version of an Isotropic Planar STIT tessellation

According to the representation formulas provided in Section 3, it is convenient to have a good understanding of the distribution of various Palm versions of the underlying STIT tessellation T in order to investigate distributional properties of typical shortest-path and total fibre lengths. In this section, we present a simulation algorithm for the Palm version $T^\times$ of T with respect to the (entire) random measure $\nu_1(\cdot\cap T^{(1)})$ and prove that this simulation algorithm yields a random tessellation with the correct distribution. We also discuss how this algorithm can be modified to generate samples of T^* and $\widetilde{T}$, see Remark 3 below.

4.1 Simulation Algorithm for $T^\times$

In [9], the construction of STIT tessellations within compact and convex sets (see Section 2.1.2) was extended to a global construction in the whole Euclidean plane $\mathbb{R}^2$. In order to give an explicit simulation algorithm for the Palm version $T^\times$ of a STIT tessellation T, large parts of this construction rule can be reused. In the following, we give a description of such an algorithm and present in greater detail those steps, which are substantially different from [9]. A formal proof for the distributional correctness of our algorithm is given in Section 4.2 below. Note that a STIT tessellation of an arbitrary length intensity $\gamma>0$ can be constructed from a STIT tessellation with length intensity 1 by applying a scaling with parameter $1/\gamma$. Hence, in the following we restrict to the case where the length intensity γ is equal to 1.

Recall that by $\mathbb{A}$, we denote the space of all lines in $\mathbb{R}^2$. This is a metric space and we write $\mathbb{K}$ for the family of all locally finite subsets of $\mathbb{A}\times[0,1]$. To construct a STIT tessellation in $\mathbb{R}^2$, one applies a deterministic construction to random input. The input data are given by a) an independently marked and motion-invariant Poisson line process $\{(\ell_n,U_n)\}_{n\geq1}$ with intensity 1 and $U_n\sim\mathrm{Uniform}([0,1])$, and b) a family of iid STIT tessellations $\{T_n\}_{n\geq1}$ with length intensity 1 which are

independent of $\{\ell_n, U_n\}_{n\geq 1}$. Then, in [9], a measurable function $\mathsf{stit} : \mathbb{K} \times \mathbb{T}^{\mathbb{N}} \to \mathbb{T}$ is defined such that a planar motion-invariant STIT tessellation can be represented as

$$\mathsf{stit}(\{(\ell_n, U_n)\}_{n\geq 1}, T_1, T_2, \ldots). \tag{7}$$

In order to retain redundant information on the one hand but not to forsake the unfamiliar reader with the notation of (7) on the other hand, we briefly describe the intuition behind this formula and go into details when giving the algorithm for the Palm version $T^{\times}$ of T. Roughly speaking, a STIT tessellation in $\mathbb{R}^2$ can be constructed in a several steps procedure. The first step is the division of the Euclidean plane into compact and convex polygons by the Poisson line process $\{(\ell_n, U_n)\}_{n\geq 1}$. Then, we consider the zero-cell of this mosaic and delete the line ℓ_n with the largest mark U_n among all lines yielding the zero-cell. This in turn arouses a zero-cell which is bigger in size. Continuing this procedure, we obtain a sequence of zero-cells with increasing area. The final step of the construction is to insert STIT tessellations $T_1, T_2, \ldots$ into the set differences (which are in fact compact and convex cells) of the zero-cells and their predecessors in the corresponding sequence of zero-cells according to Section 2.1.2 with suitable intensities.

Let us consider a further line ℓ_0 through the origin with an angle to the x-axis chosen uniformly from the interval $[0, \pi]$ and a mark $U_0 \sim \text{Uniform}([0, 1])$, and assume that they are independent and (ℓ_0, U_0) is independent of $\{(\ell_n, U_n)\}_{n\geq 1}$. We show in Theorem 3 below that the Palm version $T^{\times}$ of T can be represented as

$$\mathsf{stit}(\{(\ell_n, U_n)\}_{n\geq 1} \cup \{(\ell_0, U_0)\}, T_1, T_2, \ldots). \tag{8}$$

The tessellation yielded by (8) given its random input is obtained by the following simulation algorithm.

(I) Simulate an independently and uniformly $[0, 1]$-marked motion-invariant Poisson line process $\{(\ell_n, U_n)\}_{n\geq 1}$ with length intensity 1. With probability 1 there exists exactly one convex polygon containing the origin.

(II) Draw a random line ℓ_0 through the origin whose angle with the x-axis is chosen uniformly from the interval $[0, \pi]$ and let U_0 be a Uniform$([0, 1])$-distributed random variable, where we assume that ℓ_0 and U_0 are independent and (ℓ_0, U_0) is independent of $\{(\ell_n, U_n)\}_{n\geq 1}$. The line ℓ_0 splits ξ into two smaller convex polygons, say ξ_1 and $\xi \setminus \xi_1$, see Figure 4 on the left.

(III) Determine the line ℓ_i with the largest mark U_i among all lines defining the boundary of ξ_1. This mark will be denoted by σ_1 in the following. Then, remove ℓ_i from $\{\ell_n\}_{n\geq 1} \cup \{\ell_0\}$. The lines $\{\ell_n\}_{n\geq 1} \cup \{\ell_0\} \setminus \{\ell_i\}$ yield a new tessellation with
   - either one cell ξ_2 containing o in its interior if $\ell_i = \ell_0$ (Figure 4 centred)
   - or two cells containing o on their boundaries if $\ell_i \neq \ell_0$ (Figure 4 on the right). In this case, choose ξ_2 such that $\xi_1 \subset \xi_2$.

(IV) Proceed with ξ_2 in an analogous way as it was done for ξ_1 in step (III). This yields the cell ξ_3 and the maximal mark σ_2. Continuing this way, we obtain a sequence of 'quasi' zero-cells $\{\xi_n\}_{n\geq 1}$ ('quasi' since o can be located on the boundary of ξ_n) and marks $\{\sigma_n\}_{n\geq 1}$.

(V) By means of $\{\xi_n\}_{n\geq 1}$, we can construct $\{\psi_n\}_{n\geq 1}$ where $\psi_1 = \xi_1$ and $\psi_n = \xi_n \setminus \xi_{n-1}$ for $n \geq 2$.

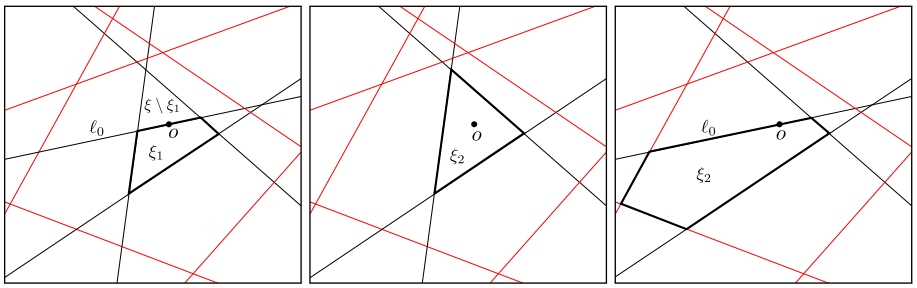

Fig. 4 Realisation of ξ_1 (left) resulting from black lines and ξ_2 where $\ell_i = \ell_0$ (centre) and $\ell_i \neq \ell_0$ (right)

(VI) Finally, each cell ψ_n with $n > 1$ is subdivided further according to the STIT tessellation $T_n' + x_n$ where x_n denotes the centre of gravity of ψ_n and T_n' is the thinning of T_n consisting of all edges with mark at most $1 - \sigma_n$.

Note that the origin is contained on the boundary of ψ_1 and therefore lies on the edge set of the constructed tessellation.

4.2 Representation of Palm Distribution

The following theorem provides a description for the Palm distribution with respect to the one-dimensional Hausdorff measure on the edge set of a motion-invariant STIT tessellation T in $\mathbb{R}^2$.

Theorem 3 *The distribution of the tessellation*

$$T_{\ell_0,U_0} = \mathsf{stit}(\{(\ell_n, U_n)\}_{n\geq 1} \cup \{(\ell_0, U_0)\}, \Xi_1, \Xi_2, \ldots) \tag{9}$$

coincides with the Palm distribution with respect to the one-dimensional Hausdorff measure on the edge set of a motion-invariant planar STIT tessellation T with $\gamma = 1$.

Remark 3 Note that if one wants to consider the Palm versions $\widetilde{T}$ and T^* of T with respect to the one-dimensional Hausdorff measure on $T_L^{(1)}$ and $T_H^{(1)}$, one has to choose $U_0 \sim \text{Uniform}([\gamma^H + \gamma^I, \gamma])$ and $U_0 \sim \text{Uniform}([0, \gamma^H))$, respectively.

Before presenting a detailed proof of Theorem 3, we provide a rough explanation for the intuition underlying the representation given in (8). Note that for every $\varepsilon > 0$, we have

$$\mathbb{E} f(T^{\times}) = \frac{1}{\pi\varepsilon^2}\, \mathbb{E} \int_{T^{(1)} \cap B_\varepsilon(o)} f(T - x)\, \nu_1(dx). \tag{10}$$

Here, $B_\varepsilon(o)$ denotes the disc centred at o with radius ε and $f : \mathbb{T} \to [0, \infty)$ is any measurable function. On the one hand, if $\varepsilon > 0$ is sufficiently small, then with a high probability at most one edge of the STIT tessellation intersects the disc $B_\varepsilon(o)$ and, additionally, this edge belongs to the zero-cell of the STIT tessellation. On the other hand, note that the zero-cell of the STIT tessellation

$\mathsf{stit}(\{(\ell_n, U_n)\}_{n\geq 1}, \Xi_1, \Xi_2, \ldots)$ coincides with the zero-cell of the Poisson line tessellation formed by the family of lines $\{\ell_n\}_{n\geq 1}$. Hence, it is intuitive to expect that the Palm version of the STIT tessellation can be obtained from the Palm version of the Poisson line tessellation yielded by $\{\ell_n\}_{n\geq 1}$. The Palm version of the latter tessellation in turn is obtained by simply adding a further isotropic line through the origin. This is a direct consequence of Slivnyak's theorem [1,3] for Poisson point processes. In order to make this intuition rigorous, the first step consists in showing that we can restrict to the case where at most one edge of the STIT tessellation intersects the disc $B_{4\varepsilon}(o)$, provided that $\varepsilon > 0$ is sufficiently small. Choosing the radius to be 4ε instead of ε guarantees that also for any shifted tessellation $T - x$ with $x \in B_\varepsilon(o)$, there exists at most one edge intersecting the disc $B_\varepsilon(o)$. To be more precise, define $A_\varepsilon = A_\varepsilon^{(1)} \cap A_\varepsilon^{(2)}$ as the intersection of the events $A_\varepsilon^{(1)}$ and $A_\varepsilon^{(2)}$, where

$$A_\varepsilon^{(1)} = \{T^{(1)} \cap B_{4\varepsilon}(o) = \bigcup_{n\geq 1} \ell_n \cap B_{4\varepsilon}(o)\}$$

is the event that inside the sampling window $B_{4\varepsilon}(o)$ the edge sets of the STIT tessellation and the Poisson line tessellation based on $\{\ell_n\}_{n\geq 1}$ coincide, and where

$$A_\varepsilon^{(2)} = \{\#\{n \geq 1 : \ell_n \cap B_{4\varepsilon}(o) \neq \emptyset\} \leq 1\}$$

is the event that the ball $B_{4\varepsilon}(o)$ is intersected by at most one line from the Poisson line process $\{\ell_n\}_{n\geq 1}$. In the following result, it will be convenient to compute the integral in (10) only in case that the event A_ε occurs. More precisely, we define

$$\eta_\varepsilon = \frac{1}{\pi\varepsilon^2}\,\mathbb{E}\int_{T^{(1)}\cap B_\varepsilon(o)} f(T-x)\,\mathbb{1}_{A_\varepsilon}(T-x)\,\nu_1(dx)$$

and show in Lemma 1 that we make an asymptotically negligible error when replacing $\mathbb{E}f(T^\times)$ by η_ε if $\varepsilon \to 0$.

Lemma 1 *Let $f : \mathbb{T} \to [0,\infty)$ be any bounded measurable function. Then,*

$$\lim_{\varepsilon\to 0} \eta_\varepsilon = \mathbb{E}f(T^\times).$$

Proof Without loss of generality, we may assume that f is bounded from above by 1. Let N_ε denote the number of line segments in $T^{(1)}$ that intersect $B_{8\varepsilon}(o)$. First, note that if $x \in B_\varepsilon(o)$ is such that

$$(T^{(1)} - x) \cap B_{4\varepsilon}(o) \neq \bigcup_{n\geq 1} (\ell_n - x) \cap B_{4\varepsilon}(o),$$

then there exist at least two line segments in $T^{(1)}$ that intersect $B_{8\varepsilon}(o)$, i.e., $N_\varepsilon \geq 2$. Similarly, if $x \in B_\varepsilon(o)$ is such that

$$(T^{(1)} - x) \cap B_{4\varepsilon}(o) = \bigcup_{n\geq 1} (\ell_n - x) \cap B_{4\varepsilon}(o),$$

but

$$\#\{n \geq 1 :\ (\ell_n - x) \cap B_{4\varepsilon}(o) \neq \emptyset\} \geq 2,$$

then $N_\varepsilon \geq 2$. Hence, we conclude from $\nu_1(T^{(1)} \cap B_\varepsilon(o)) \leq 2\varepsilon N_\varepsilon$ that

$$|\mathbb{E}f(T^\times) - \eta_\varepsilon| \leq \frac{1}{\pi\varepsilon^2}\,\mathbb{E}\,\nu_1(T^{(1)} \cap B_\varepsilon(o))\mathbb{1}_{N_\varepsilon \geq 2}(T) \leq \frac{2}{\pi\varepsilon}\,\mathbb{E}N_\varepsilon \mathbb{1}_{N_\varepsilon \geq 2}(T),$$

We assert that $\varepsilon^{-1}\,\mathbb{E}N_\varepsilon \mathbb{1}_{N_\varepsilon \geq 2}$ tends to 0 as $\varepsilon \to 0$. The event $\{N_\varepsilon \geq 2\}$ describes a STIT tessellation such that the disc $B_{8\varepsilon}(o)$ is first subdivided into two cells and then at least one of these cells is again subdivided by at least one segment of the STIT tessellation. Using the construction of the STIT tessellation provided in [11], the probability that there exists one edge of the STIT tessellation intersecting the ball $B_{8\varepsilon}(o)$ is given by $1 - \exp(-16\varepsilon) \leq 16\varepsilon$. Furthermore, conditioned on the existence of this edge, the ball $B_{8\varepsilon}(o)$ is subdivided into two cells W^+ and W^-, and again the probability that W^+ is intersected by a further edge of the STIT tessellation is at most 16ε. Since the same is true for W^-, we obtain that $\mathbb{P}(N_\varepsilon \geq 2) \leq 512\varepsilon^2$. Finally, conditioned on $\{N_\varepsilon \geq 2\}$, the expected number of I-segments of the STIT tessellation that intersect $B_{8\varepsilon}(o)$ is at most $2 + 3\mathbb{E}N_\varepsilon \leq 2 + 3\mathbb{E}N_1$. Indeed, the first two segments partition $B_{8\varepsilon}(o)$ into three parts each of which is subdivided according to a suitable STIT tessellation. Hence, $\varepsilon^{-1}\,\mathbb{E}N_\varepsilon \mathbb{1}_{N_\varepsilon \geq 2} \leq 512\varepsilon(2 + 3\mathbb{E}N_1)$, which completes the proof of the lemma.

Note that

$$\begin{aligned}
&\mathbb{E}\int_{T^{(1)}\cap B_\varepsilon(o)} f(T-x)\,\mathbb{1}_{A_\varepsilon}(T-x)\,\nu_1(dx)\\
=\;&\mathbb{E}\mathbb{1}_{A_\varepsilon^+}(T)\int_{T^{(1)}\cap B_\varepsilon(o)} f(T-x)\,\mathbb{1}_{A_\varepsilon}(T-x)\,\nu_1(dx)\\
&+\mathbb{E}\mathbb{1}_{A_\varepsilon^-}(T)\int_{T^{(1)}\cap B_\varepsilon(o)} f(T-x)\,\mathbb{1}_{A_\varepsilon}(T-x)\,\nu_1(dx),
\end{aligned}$$

where A_ε^+ (A_ε^-) is the event that all lines intersecting $B_\varepsilon(o)$ have their perpendicular foot in the upper (lower) half-plane of $\mathbb{R}^2$. Any such line can be represented as $r_\rho(\mathbb{R}e_1 + se_2)$ for some $\rho \in [-\pi/2, \pi/2]$ ($\rho \in [\pi/2, 3\pi/2]$) and $s \in [0, \varepsilon]$, where $r_\rho : \mathbb{R}^2 \to \mathbb{R}^2$ denotes rotation by the angle ρ and where we put $e_1 = (1, 0)$, $e_2 = (0, 1)$. Note that if $x \in T^{(1)} \cap B_\varepsilon(o)$ is such that $T - x \in A_\varepsilon$, then there exists precisely one line intersecting $B_\varepsilon(o)$. Using the Slivnyak-Mecke formula [1,3], we obtain that

$$\begin{aligned}
\eta_\varepsilon =\;&\frac{1}{\pi\varepsilon^2}\,\mathbb{E}\mathbb{1}_{A_\varepsilon^+}(T)\sum_{n\geq 1}\int_{\ell_n\cap B_\varepsilon(o)} f(T-x)\,\mathbb{1}_{A_\varepsilon}(T-x)\,\nu_1(dx)\\
&+\frac{1}{\pi\varepsilon^2}\,\mathbb{E}\mathbb{1}_{A_\varepsilon^-}(T)\sum_{n\geq 1}\int_{\ell_n\cap B_\varepsilon(o)} f(T-x)\,\mathbb{1}_{A_\varepsilon}(T-x)\,\nu_1(dx)\\
=\;&\frac{1}{\pi^2\varepsilon^2}\int_{-\pi/2}^{\pi/2}\int_0^\varepsilon\int_0^1\int_{r_\rho(\mathbb{R}e_1+se_2)\cap B_\varepsilon(o)} g_\varepsilon(x, r_\rho(\mathbb{R}e_1+se_2), u)\,\nu_1(dx)\,du\,ds\,d\rho,\\
&+\frac{1}{\pi^2\varepsilon^2}\int_{\pi/2}^{3\pi/2}\int_0^\varepsilon\int_0^1\int_{r_\rho(\mathbb{R}e_1+se_2)\cap B_\varepsilon(o)} g_\varepsilon(x, r_\rho(\mathbb{R}e_1+se_2), u)\,\nu_1(dx)\,du\,ds\,d\rho,
\end{aligned}$$

where for $(\ell, u) \in \mathbb{A} \times [0, 1]$ and $x \in \ell$, we put

$$g_\varepsilon(x, \ell, u) = \mathbb{E}f(T_{\ell,u} - x)\,\mathbb{1}_{T^{(1)}_{\ell,u}\cap B_{4\varepsilon}(x) = \ell\cap B_{4\varepsilon}(x)}.$$

For the second equality, we used that the intensity measure of the Poisson line process is given as the product measure of the uniform distribution on $[0, 2\pi)$ and the Lebesgue measure on $\mathbb{R}$. Note that by stationarity, $g_\varepsilon(x, \ell, u) = g_\varepsilon(o, \ell', u)$, where $\ell' = \ell - x$ denotes the line through the origin o with the same slope as ℓ. Therefore,

$$\begin{aligned}\eta_\varepsilon &= \frac{2}{\pi^2\varepsilon^2}\int_{-\pi/2}^{\pi/2}\int_0^\varepsilon\int_0^1 2\sqrt{\varepsilon^2 - s^2}\, g_\varepsilon(o, r_\rho(\mathbb{R}e_1), u)\, du\, ds\, d\rho \\ &= \frac{1}{\pi}\int_{-\pi/2}^{\pi/2}\int_0^1 g_\varepsilon(o, r_\rho(\mathbb{R}e_1), u)\, du\, d\rho.\end{aligned}$$

Hence, it remains to show that, as $\varepsilon \to 0$, the latter expression tends to

$$\frac{1}{\pi}\int_{-\pi/2}^{\pi/2}\int_0^1 \mathbb{E}f(T_{r_\rho(\mathbb{R}e_1),u})\, du\, d\rho.$$

This convergence is shown in the following lemma.

Lemma 2 *It holds that*

$$\lim_{\varepsilon\to 0}\eta_\varepsilon = \frac{1}{\pi}\int_{-\pi/2}^{\pi/2}\int_0^1 \mathbb{E}f(T_{r_\rho(\mathbb{R}e_1),u})\, du\, d\rho.$$

Proof Indeed, we have

$$\begin{aligned}&\Big|\eta_\varepsilon - \frac{1}{\pi}\int_{-\pi/2}^{\pi/2}\int_0^1 \mathbb{E}f(T_{r_\rho(\mathbb{R}e_1),u})\, du\, d\rho\Big| \\ &\quad= \frac{1}{\pi}\int_{-\pi/2}^{\pi/2}\int_0^1 \mathbb{E}f(T_{r_\rho(\mathbb{R}e_1),u})\mathbb{1}_{T^{(1)}_{r_\rho(\mathbb{R}e_1),u}\cap B_{4\varepsilon}(o)\neq r_\rho(\mathbb{R}e_1)\cap B_{4\varepsilon}(o)}\, du\, d\rho,\end{aligned}$$

so that by dominated convergence it suffices to show that almost surely,

$$\lim_{\varepsilon\to 0}\mathbb{1}_{T^{(1)}_{r_\rho(\mathbb{R}e_1),u}\cap B_{4\varepsilon}(o)=r_\rho(\mathbb{R}e_1)\cap B_{4\varepsilon}(o)} = 1.$$

This identity is a consequence of the local finiteness of $T^{(1)}_{r_\rho(\mathbb{R}e_1),u}$.

Combining Lemmas 1 and 2, we can now complete the proof of Theorem 3, since

$$\mathbb{E}f(T^\times) = \lim_{\varepsilon\to 0}\eta_\varepsilon = \frac{1}{\pi}\int_{-\pi/2}^{\pi/2}\int_0^1 \mathbb{E}f(T_{r_\rho(\mathbb{R}e_1),u})\, du\, d\rho.$$

5 Numerical Results

In the present section, the outcomes of some numerical investigations for the cost functionals introduced in Section 3 are provided. The simulations are based on the Palm version of the STIT tessellation which was derived in Section 4. To be more precise, the new description of the Palm version is used as follows. In Corollary 1, we have seen that the density of shortest-path lengths can be estimated by performing suitable Monte Carlo simulations with respect to the Palm distribution of HLC. Moreover, as explained in Section 2.4.1, this Palm distribution can also be recovered by first considering the Palm distribution of the underlying tessellation and then adding a suitable Cox point process on its edge set. Although Section 2.4.1 deals with LLC, these remarks are of general nature and remain true for HLC.

5.1 Typical Shortest-path Lengths

We study numerically the behaviour of various typical distances in fixed-access networks based on several choices of the parameters which determine the network. Assume that we have an iid sample $\{S_L^{*,1}, \ldots, S_L^{*,n}\}$ of S_L^*. Then, we can use Corollary 1 and replace the expectations in (3) and (4) by the corresponding arithmetic means of functionals based on S_L^*, $R_{L,i}^*$ and Z_i^*. Thus, Monte Carlo estimators for the densities of $\widetilde{C}_{LH}$ and $\widetilde{C}_{LIH}$ are given by

$$\widehat{f}_{\widetilde{C}_{LH}}(x) = \frac{1}{\sum_{k=1}^n \nu_1\big(S_L^{*,k}\big)} \sum_{k=1}^n f'_{S_L^{*,k}}(x, o) \tag{11}$$

as well as

$$\widehat{f}_{\widetilde{C}_{LIH}}(x) = \frac{1}{\sum_{k=1}^n \nu_1\big(S_L^{*,k}\big)} \sum_{k=1}^n \sum_{i=1}^M f'_{R_{L,i}^{*,k}}(x, Z_i^{*,k}). \tag{12}$$

Note that for an unfavourable choice of the network parameters, the estimation procedure for the densities becomes very time-consuming. Thus, from the application point of view, there is a great interest in fitting commonly used parametric density functions to (11) and (12) whose parameters depend on the network parameters. One suitable tool is the well-known maximum-likelihood method. It turns out that approximately we have

$$\widetilde{C}_{LH} \sim \text{Gamma}(k, \lambda) \quad \text{and} \quad \widetilde{C}_{LIH} \sim \text{Gamma}(k', \lambda') \tag{13}$$

for some shape parameters $k, k' \in [0, \infty)$ and scale parameters $\lambda, \lambda' \in [0, \infty)$. Here, the density function $f_X(x)$ of a gamma-distributed random variable X with parameters $\ell, \varphi > 0$ is given by

$$f_X(x) = \frac{x^{\ell-1}\exp(-x/\varphi)}{\varphi^\ell \Gamma(\ell)} \, \mathbb{1}_{(0,\infty)}(x),$$

where $\Gamma(\cdot)$ denotes the gamma function. In Figure 5, the empirical density functions $\widehat{f}_{\widetilde{C}_{LH}}$ (black) and $\widehat{f}_{\widetilde{C}_{LIH}}$ (gray) are plotted together with their fitted parametric density functions of the corresponding gamma distributions (dashed in red and blue, respectively) for different choices of network parameters ($n = 5000$, $\gamma^H = \gamma^I = \gamma^L = 0.0005$, $\lambda_\ell^H = \lambda_\ell^I = \lambda_\ell^L = 0.00075$ on the left and $\gamma^H = \gamma^I = \gamma^L = 1/300$, $\lambda_\ell^H = \lambda_\ell^I = \lambda_\ell^L = 0.0005$ on the right). Note that $\widetilde{C}_{LH}$ is stochastically smaller than $\widetilde{C}_{LIH}$ since we do not have to make a detour via an intercomposed node between LLC and HLC which may be indeed the case for $\widetilde{C}_{LIH}$. This stochastic ordering is also reflected in Figure 5, where the density functions of $\widetilde{C}_{LH}$ and $\widetilde{C}_{LIH}$ intersect only once.

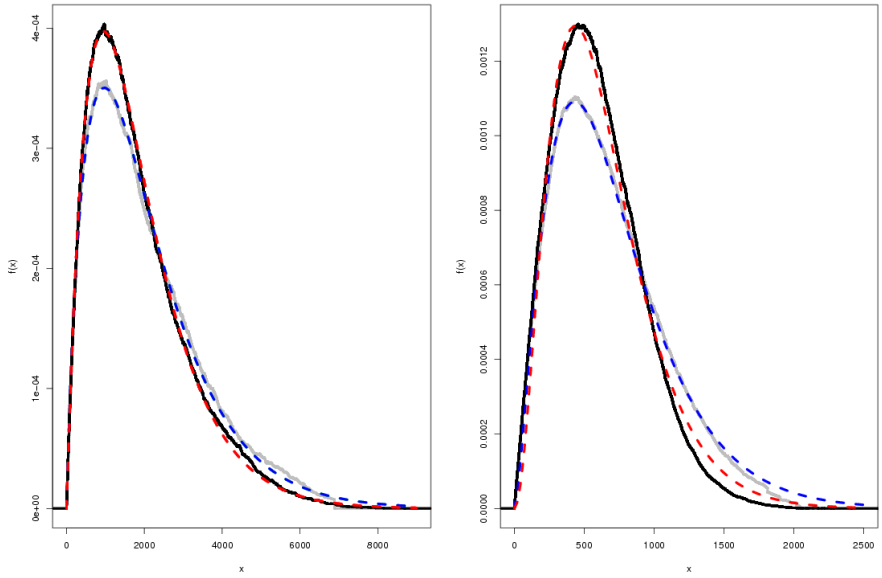

Fig. 5 Empirical density functions $\widehat{f}_{\widetilde{C}_{LH}}$ (black) and $\widehat{f}_{\widetilde{C}_{LIH}}$ (grey) together with corresponding fitted parametric densities (red and blue, respectively) for two different choices of network parameters

5.2 Typical Total Fibre Lengths

Analogously to Section 5.1, we investigate numerically the expectation of various typical total fibre lengths. Again, we consider several choices of the network parameters. The Monte Carlo estimators for the expected typical total fibre lengths $\mathbb{E}D^*_{HL}$ and $\mathbb{E}D^*_{HIL,\alpha}$ in (5) and (6) are given by

$$\mu_1 = \frac{\lambda_\ell^L}{n} \sum_{k=1}^{n} \int_{S_L^{*,k}} c(o,y)\, \nu_1(dy)$$

and

$$\mu_{2,\alpha} = \frac{1}{n} \sum_{k=1}^{n} \sum_{i=1}^{M} \left(c(o, Z_i^{*,k}) \rho_\alpha\big(\lambda_\ell^L \nu_1(R_{L,i}^{*,k})\big) + \lambda_\ell^L \int_{R_{L,i}^{*,k}} c\big(y, g(y)\big)\, \nu_1(dy) \right),$$

respectively. In Table 1, some values of μ_1 and $\mu_{2,0.7}$ for different choices of the linear intensity λ_ℓ^L are listed exemplarily. Here, we choose $\gamma^H = \gamma^I = \gamma^L = 25/30000$, $\lambda_\ell^H = \lambda_\ell^I = 0.00075$ and $n = 5000$.

The mindful reader can draw the following conclusions which are of intuitive nature. On the one hand, for increasing values of λ_ℓ^L, both quantities μ_1 and $\mu_{2,0.7}$ increase as well. On the other hand, for small values of λ_ℓ^L, μ_1 can be smaller than $\mu_{2,0.7}$ and vice versa, whereas for sufficiently large values of λ_ℓ^L, we have $\mu_{2,0.7} \leq \mu_1$, see Section 6.2.

λ_ℓ^L	μ_1	$\mu_{2,0.7}$
0.00075	1325.72	1401.59
0.0075	13638.14	11947.39
0.01	17098.46	15646.82
0.03	51916.14	44413.69

Table 1 Values of μ_1 and $\mu_{2,0.7}$ for several choices of λ_ℓ^L where $n = 5000$

6 Limit Theorems

We now provide limit theorems for the functionals defined in Section 3 if the corresponding linear intensities tend to infinity.

6.1 Typical Shortest-path Lengths

Limit theorems are an important tool to understand the behaviour of network characteristics in asymptotic scenarios. Since we have altogether six model parameters $(\gamma^H, \gamma^I, \gamma^L, \lambda_\ell^H, \lambda_\ell^I, \lambda_\ell^L)$, a large number of limiting scenarios are thinkable. Within this section, we determine the limit behaviour of the random variable $\widetilde{C}_{LH}$ in case that $\lambda_\ell^H \to \infty$. This is a regime, where the number of HLC is large. We also comment on a possible extension of this result to $\widetilde{C}_{LIH}$. Of course, these are only two possible scenarios and it would be worthwhile to investigate further limiting regimes.

Let $\widetilde{T}_H^{(1)}$ denote the subset of all edges in $\widetilde{T}$ whose mark is contained in $[0, \gamma^H]$. We define the random variable $V = \min_{x \in \widetilde{T}_H^{(1)}} c(o, x)$ as the minimal distance from the origin to a point from $\widetilde{T}_H^{(1)}$ measured along $\widetilde{T}$.

Theorem 4 *If $\lambda_\ell^H \to \infty$, then $\widetilde{C}_{LH}$ converges in distribution to V.*

Proof Note that there is a coupling between the point processes of HLC $\widetilde{X}_H = \widetilde{X}_H(\lambda_\ell^H)$ for all linear intensities λ_ℓ^H such that $\widetilde{X}_H(\lambda_\ell^H) \subset \widetilde{X}_H(\lambda_\ell'^H)$, whenever $\lambda_\ell^H \le \lambda_\ell'^H$. Recall that $\widetilde{X}_{H,o}$ denotes the closest point in the graph sense of $\widetilde{X}_H$ to the LLC in o. We show that in this coupling the random variables $\widetilde{C}_{LH} = c(o, \widetilde{X}_{H,o}(\lambda_\ell^H))$ converge to V almost surely as $\lambda_\ell^H \to \infty$. First, we note that $c(o, \widetilde{X}_{H,o}(\lambda_\ell^H))$ is decreasing in λ_ℓ^H, and the definition of V yields immediately that $\lim_{\lambda_\ell^H \to \infty} c(o, \widetilde{X}_{H,o}(\lambda_\ell^H)) \ge V$ almost surely. On the other hand, let $P \in \widetilde{T}_H^{(1)}$ be such that $c(o, P) = V$, i.e., P denotes (one of) the closest point(s) in the graph sense of the tessellation formed by the green segments to the LLC located in o, see Figure 6. Let $\varepsilon > 0$ be arbitrary. Then, provided that λ_ℓ^H is sufficiently large, $\widetilde{X}_H(\lambda_\ell^H)$ contains a point Q such that $[P, Q] \subset \widetilde{T}$ and $\nu_1([P, Q]) \le \varepsilon$. In particular, almost surely,

$$\lim_{\lambda_\ell^H \to \infty} c(o, \widetilde{X}_{H,o}(\lambda_\ell^H)) \le c(o, P) + c(P, Q) \le V + \varepsilon.$$

As $\varepsilon > 0$ was arbitrary, this completes the proof.

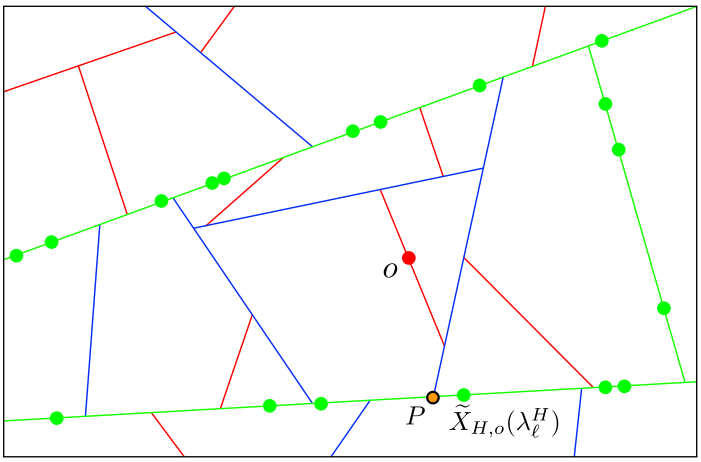

Fig. 6 Illustration of the situation with HLC (green) and LLC (red)

Remark 4 Similar arguments could be used to identify the limiting distribution of the distances $\widetilde{C}_{LIH}$. However, since additional efforts are needed to define properly the subset of $\widetilde{T}_H^{(1)}$ corresponding to the asymptotic serving zone of P, we do not provide details.

6.2 Total Fibre Lengths

Note that $\widetilde{C}_{LH} = c(o, \widetilde{X}_{H,o})$ and $\widetilde{C}_{LIH} = c(o, \Phi) + c(\Phi, \widetilde{X}_{H,o})$ are both defined on the same probability space. In particular, it holds that $\widetilde{C}_{LH}$ is stochastically smaller than $\widetilde{C}_{LIH}$, i.e. $\mathbb{P}(\widetilde{C}_{LH} \le x) \ge \mathbb{P}(\widetilde{C}_{LIH} \le x)$ for all $x > 0$. In other words, introducing an intermediate layer has on the one hand the undesirable effect of increasing typical shortest-path lengths from an LLC to its associated HLC. On the other hand, we have already seen in Section 5.2 that on the positive side, the additional layer has the potential to decrease total fibre lengths substantially. In general, this will not be true for networks, where LLC are distributed sparsely. However, in the present subsection we observe that in the dense regime where $\lambda_\ell^L \to \infty$, total fibre lengths become stochastically smaller when an intermediate level is added.

Theorem 5 *If $\lambda_\ell^L \to \infty$ and $\alpha < 1$, then D_{HL}^*/λ_ℓ^L and $D_{HIL,\alpha}^*/\lambda_\ell^L$ converge almost surely to $\int_{S_L^*} c(o,y)\nu_1(dy)$ and $\sum_{i=1}^M \int_{R_{L,i}^*} c(y, Z_i^*)\nu_1(dy)$, respectively. In particular, the asymptotic scaled total fibre length $\lim_{\lambda_\ell^L\to\infty} D_{HL}^*/\lambda_\ell^L$ is stochastically larger than $\lim_{\lambda_\ell^L\to\infty} D_{HIL,\alpha}^*/\lambda_\ell^L$.*

Proof The first limit result is an immediate consequence of the strong law of large numbers. Since $\alpha < 1$ and $\lim_{\lambda_\ell^L\to\infty} \#(R_{L,i}^* \cap \{X_{L,m}^*\})/\lambda_\ell^L = \nu_1(R_{L,i}^*)$, we conclude that $\sum_{i=1}^M c(o, Z_i)(\#(R_{L,i}^* \cap \{X_{L,m}^*\}))^\alpha/\lambda_\ell^L$ tends to 0 almost surely. Hence, a second application of the law of large numbers yields the asserted asymptotic

behaviour of $D^*_{HIL,\alpha}/\lambda_\ell^L$ as $\lambda_\ell^L \to \infty$. Finally, for the last claim we note that

$$\int_{S_L^*} c(o,y)\nu_1(dy) - \sum_{i=1}^{M} \int_{R^*_{L,i}} c(y,Z_i^*)\nu_1(dy) = \sum_{i=1}^{M} \int_{R^*_{L,i}} c(y,o) - c(y,Z_i^*)\nu_1(dy),$$

and the right hand side is non-negative since the definition of R_i^* implies that $c(y,o) \geq c(y,Z_i^*)$ for all $y \in R_i^*$.

7 Conclusions and Outlook

The present paper provides a substantial extension of the standard SSLM which consists of just two levels of hierarchy and was thoroughly discussed for instance in [4,13,16]. More precisely, we gave a detailed description of a multi-hierarchical modelling approach for fixed-access networks. We investigated the effects on two important cost functionals caused by the introduction of an additional (intermediate) level of hierarchy. Both numerical and theoretical evidence were provided for the intuitive conjecture that in the new scenario, the typical shortest-path length increases whereas the typical total fibre length should decrease. The modelling approach is based on STIT tessellations for which the Palm version with an appropriate simulation algorithm was deduced.

Possible future work could be extending the presented scenario interposing even further network components between HLC and LLC beyond an ILC. This means that we have at least four or even more components with different kind of hierarchy in the access network. This should be a straightforward procedure. To further increase the flexibility of the model, one can additionally think of randomly choosing certain cells of the underlying STIT tessellation which are not iterated further, e.g. some kind of a Bernoulli type thinning of cells. Of course, the investigation of distributional properties of further cost functionals in fixed-access telecommunication networks can be handled as well.

References

1. Chiu S.N., Stoyan D., Kendall W.S., Mecke J. *Stochastic Geometry and its Applications*. J. Wiley & Sons, Chichester, 2013.
2. Courtat T. *Walk on City Maps – Mathematical and Physical Phenomenology of the City, a Geometrical Approach*. PhD-thesis, MSC Lab of Paris-Diderot University, Paris, 2012.
3. Daley D.J., Vere-Jones D. *An Introduction to the Theory of Point Processes*. Vol. I/II, Springer, New York, 2005/08.
4. Fleischer F., Gloaguen C., Schmidt V., Voss F. Simulation of the typical Poisson-Voronoi-Cox-Voronoi cell. *Journal of Statistical Computation and Simulation*, 79:939–957, 2009.
5. Gloaguen C., Fleischer F., Schmidt H., Schmidt V. Simulation of typical Cox-Voronoi cells, with a special regard to implementation tests. *Mathematical Methods of Operations Research*, 62:357–373, 2005.
6. Gloaguen C., Fleischer F., Schmidt H., Schmidt V. Fitting of stochastic telecommunication network models via distance measures and Monte-Carlo tests. *Telecommunication Systems*, 31:353-377, 2006.
7. Kendall W.S., Molchanov I. *New Perspectives in Stochastic Geometry*. Oxford University Press, Oxford, 2010.
8. Maier R., Mayer J., Schmidt V. Distributional properties of the typical cell of stationary iterated tessellations. *Mathematical Methods of Operations Research*, 59:287–302, 2004.

9. Mecke J., Nagel W., Weiß V. A global construction of homogeneous random planar tessellations that are stable under iteration. *Stochastics*, 80:51–67, 2008.
10. Mecke J., Nagel W., Weiß V. Some distributions for I-segments of planar random homogeneous STIT tessellations. *Mathematische Nachrichten*, 284:1483–1495, 2011.
11. Nagel W., Weiß V. Crack STIT tessellations: Characterization of stationary random tessellations stable with respect to iteration. *Advances in Applied Probability*, 37:859–883, 2005.
12. Neuhäuser D., Hirsch C., Gloaguen C., Schmidt V. Joint distributions for total lengths of shortest-path trees in telecommunication networks. *Annals of Telecommunications*, 2014 (DOI: 10.1007/s12243-014-0440-9).
13. Neuhäuser D., Hirsch C., Gloaguen C., Schmidt V. On the distribution of typical shortest-path lengths in connected random geometric graphs. *Queueing Systems*, 71:199–220, 2012.
14. Schreiber T., Thäle C. Limit theorems for iteration stable tessellations. *The Annals of Probability*, 41:2261–2278, 2013.
15. Thäle C., Redenbach C. On the arrangement of cells in planar STIT and Poisson line tessellations. *Methodology and Computing in Applied Probability*, 15:643-654, 2013.
16. Voss F., Gloaguen C., Fleischer F., Schmidt V. Densities of shortest path lengths in spatial stochastic networks. *Stochastic Models*, 27:141–167, 2011.
17. Weiss V., Ohser J., Nagel W. Second moment measure and K-function for planar STIT tessellations. *Image Analysis & Stereology*, 29:121–131, 2010.